LETTER TO THE EDITOR

CO rotational line emission from a dense knot in Cassiopeia A

Evidence for active post-reverse-shock chemistry

Sofia H. J. Wallström¹, Chiara Biscaro², Francisco Salgado³, John H. Black¹, Isabelle Cherchneff², Sébastien Muller⁴, Olivier Berné^{5,6}, Jeonghee Rho^{7,8}, and Alexander G. G. M. Tielens³

- Department of Earth and Space Sciences, Chalmers University of Technology, 43992 Onsala, Sweden e-mail: sofia.wallstrom@chalmers.se
- ² Department Physik, Universität Basel, 4056 Basel, Switzerland
- ³ Leiden Observatory, Leiden University, PO Box 9513, 2300 RA Leiden, The Netherlands
- ⁴ Onsala Space Observatory, Chalmers University of Technology, 43992 Onsala, Sweden
- Université de Toulouse, UPS-OMP, IRAP, 31028 Toulouse, France
- ⁶ CNRS, IRAP, 9 Av. Colonel Roche, BP 44346, 31028 Toulouse Cedex 4, France
- ⁷ SETI Institute, 189 N. Bernardo Ave, Mountain View, CA 94043, USA
- 8 Stratospheric Observatory for Infrared Astronomy, NASA Ames Research Center, MS 211-3, Moffett Field, CA 94035, USA

Received 30 August 2013 / Accepted 13 September 2013

ABSTRACT

We report a $Herschel^*$ detection of high-J rotational CO lines from a dense knot in the supernova remnant Cas A. Based on a combined analysis of these rotational lines and previously observed ro-vibrational CO lines, we find the gas to be warm (two components at ~400 and 2000 K) and dense (10^{6-7} cm⁻³), with a CO column density of ~5 × 10^{17} cm⁻². This, along with the broad line widths (~400 km s⁻¹), suggests that the CO emission originates in the post-shock region of the reverse shock. As the passage of the reverse shock dissociates any existing molecules, the CO has most likely reformed in the past several years in the post-shock gas. The CO cooling time is similar to the CO formation time, therefore we discuss possible heating sources (UV photons from the shock front, X-rays, electron conduction) that may maintain the high column density of warm CO.

Key words. ISM: supernova remnants – submillimeter: ISM – ISM: individual objects: Cassiopeia A

1. Introduction

Stars with masses ranging from 8 to 30 M_{\odot} have lifetimes of only $\sim \! 10^7$ years (Woosley et al. 2002) before exploding as type II supernovae (SNe), and can thus enrich their local environments on a short timescale. Dust grains and molecules are produced in the ejected material (ejecta), despite the harsh physical conditions. Emission from CO and SiO molecules has been observed at infrared (IR) wavelengths in SN1987A some hundred days after the SN explosion (Danziger et al. 1987; Lucy et al. 1989; Roche et al. 1991), and in several other SNe (Kotak et al. 2005, 2006, 2009). These observations demonstrate that a rapid and efficient chemistry develops in the ejecta, and that molecular formation is a common occurrence in SNe (Lepp et al. 1990; Cherchneff & Sarangi 2011). CO and SiO have been observed in the ejecta of SN1987A (Kamenetzky et al. 2013), demonstrating that these molecules have survived up to 25 years after the SN explosion.

SNe are prime contenders for explaining the large dust masses in the early Universe, inferred from the reddening of background quasars and Lyman- α systems at high redshift (Pei et al. 1991; Pettini et al. 1994; Bertoldi et al. 2003), because

efficient dust formation on short timescales is required. However, IR observations of SNe ~400 days post-explosion show dust masses ranging between 10^{-5} and 10^{-2} M_{\odot} (e.g., Lucy et al. 1989; Sugerman et al. 2006; Szalai & Vinkó 2013), at least an order of magnitude too low to explain the observed high-z dust (Dwek et al. 2008). Larger dust masses have been observed in supernova remnants (SNRs), for example ~0.7 M_{\odot} of cool dust in the young remnant of SN1987A (Matsuura et al. 2011). Observations of the SNR Cas A imply ~0.025 M_{\odot} of warm dust (Rho et al. 2008), and ~0.075 M_{\odot} of cool dust (Barlow et al. 2010). However, these dust masses do not necessarily represent the net SN dust yields into the ISM, as the passage of a reverse shock might reprocess the dust grains.

When a SN explosion shock wave has swept up enough circumstellar and interstellar matter, a reverse shock forms and travels inward, decelerating and reprocessing the ejecta (Chevalier 1977). At the shock front the ejecta will be heated to $>10^6$ K, sputtering dust and dissociating molecules. However, the shock can be attenuated in dense knots in the ejecta, which mitigates its destructive effects there.

The 330-year-old SNR Cas A (D=3.4 kpc) is the perfect laboratory for studying the effects of the reverse shock, because it is just beginning to reprocess the ejecta. Ro-vibrational CO emission has been detected in Cas A (Rho et al. 2009, 2012), in several (\sim 20) small (<0.8") knots coincident with the

^{*} *Herschel* is an ESA space observatory with science instruments provided by European-led Principal Investigator consortia and with important participation from NASA.

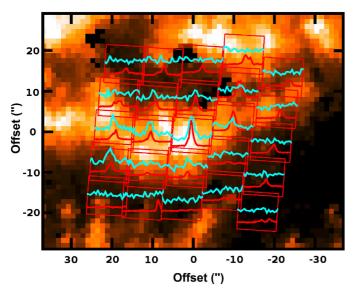


Fig. 1. PACS footprint, centered on RA 23:23:24.9 Dec +58:50:03.3, showing the spectra of CO J=23–22 in blue and [O III] 88 μ m in red, overlaid on a Spitzer/IRAC image of the CO vibrational emission in Cas A.

reverse shock. Such knots are reminiscent of the fast-moving knots (FMKs) seen in the optical (Fesen 2001). To determine the chemical and physical conditions in these knots, we used the *Herschel* PACS instrument to observe several high-*J* rotational CO lines toward the brightest CO knot in the remnant.

2. Observations

The Photodetector Array Camera and Spectrometer (PACS; Poglitsch et al. 2010) onboard the *Herschel* Space Observatory (Pilbratt et al. 2010) was used on 2012 June 11 to observe a single pointing in the northwest of Cas A (Fig. 1). PACS consists of a 5×5 array of spatial pixels (spaxels), each $9.4'' \times 9.4''$ in size. We selected seven CO rotational transitions, between $J_{\rm up}=14$ and 38 for an even coverage of the CO ladder in the PACS spectral range. The observations were made using short-range spectroscopy scans with high spectral resolution (R=1000-2700, $\sim 100-300$ km s⁻¹). The [O III] 88 μ m transition was observed within the covered spectral range. Observations were done in chopping/nodding mode with a chop throw of 6' to the north and south, well off the remnant.

The data were processed using the standard range-scan reduction pipeline, implemented in HIPE version 9.0.0 (Ott 2010). The CO J=38-37 spectrum was marred by an artifact and thus discarded. A first-degree polynomial baseline was fit from line-free channels and subtracted. The final spectra correspond to the central spaxel after applying the standard PACS point-source correction to correct for flux spill-over into adjacent spaxels. PACS has an absolute flux accuracy of ~10% (PACS Observer's Manual).

3. Results

All the targeted CO lines were detected in the central PACS spaxel. The line profiles extracted from the central spaxel (Fig. 2) were fit with Gaussians (Table 1). The lines have an average radial velocity of -2740 km s⁻¹, consistent with the velocity of the IR knot n2 (Rho et al. 2012, close to our target position),

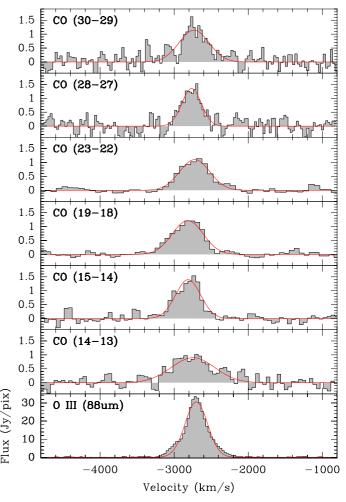


Fig. 2. CO and O III emission lines in velocity (LSR), with Gaussian fits, extracted from the central PACS spaxel. Note that the flux density scale is different for the O III line.

Table 1. Data of the CO and [O III] lines extracted from the central spaxel.

Line	λ	v_0	δv	∫Flux dv
	$\mu\mathrm{m}$	${ m km}{ m s}^{-1}$	${ m km~s^{-1}}$	$10^{-18}~{\rm W}~{\rm m}^{-2}$
CO (14-13)	186.00	-2882(370)	661(63)	35(2)
CO (15-14)	173.63	-2814(362)	336(24)	34(2)
CO (19-18)	137.20	-2814(336)	409(19)	46(2)
CO (23-22)	113.46	-2716(309)	372(19)	50(2)
CO (28-27)	93.35	-2765(105)	292(32)	48(4)
CO (30-29)	87.19	-2733(470)	418(46)	64(6)
[OIII]	88.36	-2701(100)	341(7)	1310(20)

Notes. v_0 is the radial velocity of the line and δv the velocity full width at half maximum. Errors are given in parentheses.

and are broad, with a deconvolved full width at half maximum of \sim 400 km s⁻¹.

The integrated CO line fluxes were used to create a rotational diagram (Goldsmith & Langer 1999), as shown in Fig. 3. We adopted a source diameter of 0.5" (much smaller than the spaxel size), consistent with the 0.8" upper limit on the near-IR ro-vibrational CO source size (Rho et al. 2009) and optical observations of FMKs (Fesen 2001). Assuming local thermal equilibrium (LTE) conditions, we derived a column density of $N_{\rm CO} = (4.1 \pm 0.3) \times 10^{17}$ cm⁻² and a rotation temperature

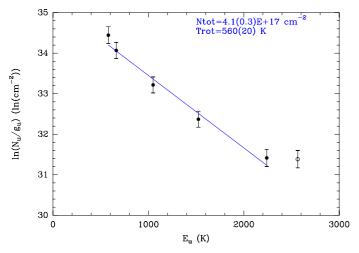


Fig. 3. CO excitation diagram, plotting $\ln (N_u/g_u)$ vs. E_u . The column density, N_{tot} , and rotation temperature, T_{rot} , and their uncertainties were calculated with a Monte Carlo method, excluding the last point; the blue line corresponds to the best-fit parameters.

of $T_{\rm rot} = 560 \pm 20$ K. This corresponds to a CO mass of $\sim 5 \times 10^{-6}~M_{\odot}$ for the knot, which is independent of the assumed knot size, because $N_{\rm CO}$ is inversely proportional to the knot size squared.

In the spectra of the full PACS footprint (Fig. 1) we see that the central spaxel emission has spilled over into the adjacent spaxels, because the point spread function is larger than the spaxel size. There is also some additional CO emission at the eastern edge of the footprint. This is most likely indicative of a second knot and not of extended CO emission, given the IR and optical evidence for a multitude of small, dense knots. Due to the increased uncertainty at the edge of the PACS footprint and the lower CO fluxes, we did not attempt to analyze this emission. In contrast to the CO emission, the emission of the [O III] line is extended across the PACS footprint, which might be explained by its critical density, which is lower than that of the high-J CO lines.

4. Discussion

To investigate the physical conditions in the knot in more detail, we analyzed the CO excitation with the non-LTE radiative transfer code RADEX (van der Tak et al. 2007), assuming a uniform emitting region (i.e., constant density, temperature, and abundance). To fit all our rotational lines as well as the previously reported ro-vibrational emission from the same region (Rho et al. 2009, 2012), multiple temperature components are required: an ~400 K component and an additional ~2000 K component, containing about 15% of the CO, to explain the ro-vibrational fluxes (shown in Fig. 4). This hot component also contributes substantially to the high-*J* rotational lines. The multiple temperature components are suggestive of the structure of a post-shock cooling zone (Borkowski & Shull 1990).

The non-LTE analysis yields $N_{\rm CO} \sim 5 \times 10^{17}$ cm⁻², similar to the rotation diagram result. The required density of the main collision partner is $\sim 10^6$ cm⁻³. Because the knot is expected to be oxygen-rich, with its strong [O III] emission and similarity to optical FMKs, we consider oxygen to be the main collision partner in this knot. However, collisional rates with CO have only been studied with H/H₂ and H₂O as collision partners. Hence, these rates were used as proxies for the unknown O + CO collisional rates. The derived density differs by

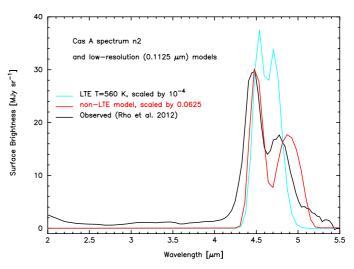


Fig. 4. Mid-IR AKARI spectrum reported by Rho et al. (2012) for knot n2 in Cas A is compared with models that have been convolved to the same resolution, $0.1125~\mu m$. The black curve is the observed spectrum. The red curve is the computed spectrum for the same two-component non-LTE model that best describes the fluxes of the CO rotational lines, but scaled in intensity by a factor 1/16. The cyan curve represents the vibrational emission expected in strict LTE for the column density and temperature derived from the rotation diagram in Fig. 3, but scaled down by a factor of 10^{-4} . The computed spectra include more than 4000 vibration-rotation lines, each of which has a width of 415 km s⁻¹.

an order of magnitude depending on the chosen collision partner. On the other hand, the critical densities of the observed CO lines are $\sim\!10^{6-7}$ cm $^{-3}$, constraining the gas density to be fairly high. The RADEX analysis indicates that the observed CO lines are optically thin ($\tau<10^{-2}$). Overall, the non-LTE analysis results are consistent with the simple rotational diagram analysis.

The high temperature and density of the CO along with the broad (\sim 400 km s⁻¹) lines suggests that the CO emission originates in a dense knot in the post-shock region of the reverse shock. In a dense knot, the reverse shock is attenuated due to energy conservation. Following Docenko & Sunyaev (2010), a 2000 km s⁻¹ reverse shock will be slowed to 200 km s⁻¹ when crossing a knot 100 times denser than the interclump medium. For a 200 km s⁻¹ shock, the gas temperature at the shock front reaches some 10^7 K, and pre-existing molecules, including CO, will be destroyed. However, ongoing chemical modeling suggests that under the observed post-shock conditions, CO will reform on a timescale of $t_{\rm CO} \sim 100$ days through radiative association reactions (Biscaro & Cherchneff, in prep.).

Shock attenuation in dense knots also has implications for the survival of SN-produced dust. A slow shock may sputter <50% of the dust mass (Silvia et al. 2012), and the warm dense gas we see in the post-shock region is conducive to grain growth. Hence, some SN dust may survive the passage of the reverse shock in dense knots.

A minimum cooling flux, $\Lambda_{\rm min}$, can be estimated from the energy radiated by the observed [O III] and CO lines in our knot. The [O III] 88 μ m line provides \sim 1 erg cm⁻² s⁻¹ of cooling, similar to that of the total rotational CO line emission, giving $\Lambda_{\rm min} \sim 2$ erg cm⁻² s⁻¹. Using a gas column density of 5×10^{19} cm⁻², as explained below, we can calculate an approximate gas cooling time ($t_{\rm cool} = N_{\rm gas}k_{\rm B}T/\Lambda_{\rm min}$) of 70 days. This is similar to the CO formation timescale $t_{\rm CO} \sim 100$ days, indicating that a constant heating flux on the order of $\Lambda_{\rm min}$ may be required to maintain the observed high column density of warm CO.

One heat source is the shock front itself, which emits UV photons. For a flux of $F_0 = n_0 \times v_s$ ($n_0 =$ oxygen density; $v_s =$ shock velocity) oxygen atoms flowing into the shock, the total UV photon flux at the surface of the knot is $30 F_0$ photons cm⁻² s⁻¹ (Borkowski & Shull 1990, Table 11). With a typical photon energy of 20 eV, we derive a heating flux of ~2 erg cm⁻² s⁻¹, similar to $\Lambda_{\rm min}$. However, the penetration depth of the UV photons is only ~3 × 10^{17} cm⁻² (Borkowski & Shull 1990), while the derived O III column density is ~ 10^{19} cm⁻². In addition, $N_{\rm CO} \sim 5 \times 10^{17}$ cm⁻² implies a gas column density of at least 5×10^{19} cm⁻², as the pre-shock CO abundance in such a knot is expected to be ~ 10^{-2} (Sarangi & Cherchneff 2013). Hence, the UV photons cannot penetrate the full gas column, and additional heating sources must be considered.

The reverse shock traveling through the tenuous inter-knot ejecta creates a hot plasma that will slowly cool through X-rays. Taking the average observed X-ray luminosity over the remnant, $5.5\times10^{37}~\text{erg s}^{-1}$ (Hartmann et al. 1997), with a typical photon energy of $\sim\!2$ keV, we obtain an X-ray heating flux of 0.2 $\text{erg cm}^{-2}\,\text{s}^{-1}$ at the knot. While the keV photons might ionize and heat a higher column density ($\sim\!3\times10^{19}~\text{cm}^{-2}$) than the UV photons, the X-ray heating flux falls short of Λ_{min} by an order of magnitude.

Heat conduction from the inter-knot hot, tenuous plasma into the dense knot might provide another heating source. The classical expression for heat conduction by electrons gives Q =K(T) dT/dr, where K(T) is approximately constant and $\sim 6 \times 10^{-7} \times T^{5/2}$ erg s⁻¹ K^{-7/2} cm⁻¹ (Tielens 2005, p. 448–449). Setting the temperature gradient equal to $T/\delta R$ with the temperature $T = 10^7$ K and the length scale δR given by the gas column density divided by the gas density, $N/n = 5 \times 10^{13}$ cm, we find an energy flux of $\sim 4 \times 10^4$ erg cm⁻² s⁻¹, which will be balanced by mass evaporation from the knot surface. The energy radiated away through the CO lines is then of little relevance for the energy budget. For the adopted parameters, the mean free path for electrons ($\sim 10^{12}$ cm) is short compared with the size scale for the temperature gradient (5×10^{13} cm), as required by the classical heat conduction expression. Though the heat flux conducted inward by electrons may be limited somewhat by magnetic fields, still heat conduction may be the key to maintaining the high column density of warm gas.

In conclusion, *Herschel* observations of rotational CO lines in a dense knot in Cas A indicate a high column density ($N_{\rm CO} \sim 5 \times 10^{17}~{\rm cm}^{-2}$) of warm (two components at ~400 and 2000 K) and dense ($10^{6-7}~{\rm cm}^{-3}$) gas in the post-shock region of the reverse shock. The passage of the shock

will dissociate any existing molecules and hence the CO has most likely been reformed recently, in the post-shock gas, providing evidence of an active chemistry in the post-reverse-shock region. The observed high column density of warm CO indicates that the cooling through CO (and ionic) lines is balanced by a constant heating flux. The diffuse X-ray flux is insufficient, and the UV photons from the shock front cannot penetrate the full gas column; accordingly, heat conduction by electrons may be required to maintain the temperature of the gas.

Acknowledgements. S.W. and C.B. thank the ESF EuroGENESIS programme for financial support through the CoDustMas network.

References

Barlow, M. J., Krause, O., Swinyard, B. M., et al. 2010, A&A, 518, 138 Bertoldi, F., Carilli, C. L., Cox, P., et al. 2003, A&A, 406, 55 Borkowski, K. J., & Shull, M. J. 1990, ApJ, 348, 169 Cherchneff, I., & Sarangi, A. 2011, IAU Symp., 280, 22 Chevalier, R. 1977, ARA&A, 15, 175 Danziger, I. J., Fosbury, R. A. E., Alloin, D., et al. 1987, A&A, 177, L13 Docenko, D., & Sunyaev, R. A. 2010, A&A, 509, 59 Dwek, E., Arendt, R. G., Bouchet, P., et al. 2008, ApJ, 676, 1029 Fesen, R. A. 2001, ApJS, 133, 161 Goldsmith, P. F., & Langer, W. D. 1999, ApJ, 517, 209 Hartmann, D. H., Predehl, P., Greiner, J., et al. 1997, Nucl. Phys. A, 621, 83 Kamenetzky, J., McCray, R., Indebetouw, R., et al. 2013, ApJ, 773, 34 Kotak, R., Meikle, P., van Dyk, S. D., et al. 2005, ApJ, 628, L123 Kotak, R., Meikle, P., Pozzo, M., et al. 2006, ApJ, 651, L117 Kotak, R., Meikle, W. P. S., Farrah, D., et al. 2009, ApJ, 704, 306 Lepp, S., Dalgarno, A., & McCray, R. 1990, ApJ, 358, 262 Lucy, L. B., Danziger, I. J., Gouiffes, C., & Bouchet, P. 1989, in Structure and Dynamics of the Interstellar Medium, IAU Colloq. 120, eds. G. Tenorio-Tagle, M. Moles, & J. Melnick, 164 Matsuura, M., Dwek, E., Meixner, M., et al. 2011, Science, 333, 1258 Ott, S. 2010, ASP Conf. Ser., 434, 139 Pei, Y. C., Fall, S. M., & Bechtold, J. 1991, ApJ, 378, 6 Pettini, M., Smith, L. J., Hunstead, R. W., & King, D. L. 1994, MNRAS, 394, Pilbratt, G., Riedinger, J., Passvogel, T., et al. 2010, A&A, 518, L1 Poglitsch, A., Waelkens, C., Geis, N., et al. 2010, A&A, 518, L2 Rho, J., Kozasa, T., Reach, W. T., et al. 2008, ApJ, 673, 271 Rho, J., Jarrett, T. H., Reach, W. T., et al. 2009, ApJ, 693, 39 Rho, J., Onaka, T., Cami, J., & Reach, W. T. 2012, ApJ, 747, 6 Roche, P. F., Aitken, D. K., & Smith, C. H. 1991, MNRAS, 252, 39 Sarangi, A., & Cherchneff, I. 2013, ApJ, in press Silvia, D. W., Smith, B. D., & Shull, J. M. 2012, ApJ, 748, 12 Sugerman, B. E. K., Ercolano, B., Barlow, M. J., et al. 2006, Science, 313, 196

Tielens, A. G. G. M. 2005, The Physics and Chemistry of the Interstellar Medium

van der Tak, F. F. S., Black, J. H., Schier, F. L., et al. 2007, A&A, 468, 627

Woosley, S. E., Heger, A., & Weaver, T. A. 2002, RvMP, 74, 1015

Szalai, T., & Vinkó, J. 2013, A&A 549, A79

(Cambridge University Press)